

A Fully Automated Platform for Evaluating ReRAM Crossbars

Rebecca Pelke*, Felix Staudigl*, Niklas Thomas*, Nils Bosbach*, Mohammed Hossein*, Jose Cubero-Cascante*, Leticia Bolzani Poehls†, Rainer Leupers*, and Jan Moritz Joseph*

**Institute for Communication Technologies and Embedded Systems, RWTH Aachen University*

†*Chair of Integrated Digital Systems and Circuit Design, RWTH Aachen University*

{pelke, staudigl, thomas, bosbach, hossein, cubero, leupers, joseph}@ice.rwth-aachen.de

poehls@ids.rwth-aachen.de

Abstract—Resistive Random Access Memory (ReRAM) is a promising candidate for implementing Computing-in-Memory (CIM) architectures and neuromorphic circuits. ReRAM cells exhibit significant variability across different memristive devices and cycles, necessitating further improvements in the areas of devices, algorithms, and applications. To achieve this, understanding the stochastic behavior of the different ReRAM technologies is essential. The NeuroBreakoutBoard (NBB) is a versatile instrumentation platform to characterize Non-Volatile Memories (NVMs). However, the NBB itself does not provide any functionality in the form of software or a controller. In this paper, we present a control board for the NBB able to perform reliability assessments of 1T1R ReRAM crossbars. In more detail, an interface that allows a host PC to communicate with the NBB via the new control board is implemented. In a case study, we analyze the Cycle-to-Cycle (C2C) variation and read disturb TiN/Ti/HfO₂/TiN cells for different read voltages to gain an understanding of their operational behavior.

Index Terms—ReRAM, Test Automation, ReRAM variability

I. INTRODUCTION

There is an ever-growing demand for efficient Neural Network (NN) inference. Due to the computationally and data-intensive workloads, traditional computers quickly encounter the von Neumann bottleneck [1] and the memory-wall [2]. One possible solution for addressing this problem is the adoption of Computing-in-Memory (CIM) architectures. The concept involves statically storing the weights of NNs in non-volatile CIM cells. The computations take place within the memory, tackling the challenges of traditional computing architectures [3], [4]. Resistive Random Access Memory (ReRAM) is a promising candidate for CIM due to its high device density, scalability, switching performance, low power consumption, and Complementary Metal-Oxide Semiconductor (CMOS) manufacturing process compatibility [5]–[7].

The downside of ReRAM is poor uniformity between cycles and devices, known as Cycle-to-Cycle (C2C) and Device-to-Device (D2D) variabilities [8]. C2C variation is associated with the stability and reliability of ReRAM devices over repeated cycles of use. It is an intrinsic property of the technology [9], [10]. D2D variation is associated with manufacturing and production consistency. Manufacturing deviations in

thickness, length, width, and surface roughness of the ReRAM cells increase the D2D variation [11]. Note that these problems prevent the rapid commercialization and adoption of ReRAM for implementing emerging applications. To advance ReRAM technology, there are several topics to explore, including

- 1) enhancing ReRAM devices [12]–[14].
- 2) improving program and read algorithms [15]–[17].
- 3) increasing the fault tolerance of applications [18]–[20].

Regardless of the topic, understanding the characteristics of individual devices is essential for properly implementing and optimizing these emerging applications. Thus, automated measurement processes are required to reduce the need for manual and time-consuming laboratory measurements. Different systems have been developed for this purpose [21]–[24], such as the NeuroBreakoutBoard (NBB). The NBB can measure a wider range of devices due to its flexibility [24].

The flexibility is achieved through a combination of the interconnect matrix, custom-designed TransImpedance Amplifiers (TIAs), and the omission of already-fixed control mechanisms on the NBB. This means that the components of the NBB need to be controlled by an external device because the NBB itself is not yet a fully functional measurement system. We aim to close this gap by developing a new platform able to perform reliability assessments of 1T1R ReRAM crossbars. In this context, the main contributions of this paper are:

- Development of a controller board that allows controlling the NBB from a host PC, eliminating the need for supervision during measurements (increase of measurement consistency and time savings in the laboratory).
- Implementation of a new interface accessible from the host PC for easily configuring the target experiments.
- Validation of the proposed controller board and interface based on a case study aiming the analysis of read voltage impact on C2C variability and read disturb of TiN/Ti/HfO₂/TiN cells.

The paper is organized as follows: Section II provides the required background related to ReRAMs' behavior as well as summarizes the main metrics adopted for evaluating ReRAM cells. Section III describes the proposed controller board and interface. Section IV summarizes the results related to the performed case study's reliability assessment. Finally, Section V draws a conclusion.

This work was partially funded by the Federal Ministry of Education and Research (BMBF, Germany) in the project NeuroSys (Project Nos. 03ZU1106CA) and NEUROTEC (project Nos. 16ES1134 and 16ES1133K).

II. STRUCTURE

This Section presents the background related to memristive devices. It further introduces their main evaluation metrics.

Memristive Devices: Structure and Functionality

A memristive device is composed of a transition-metal-oxide layer, e.g., HfO_2 , ZrO_2 , Ta_2O_5 , or TiO_2 , between two conducting electrodes [5]. After manufacturing, especially in oxide-based filamentary-type devices, memristive devices usually have very high electrical resistance. A large voltage is required for the very first *set* operation, also known as the *forming* process [25]. This process, a controlled soft breakdown, drastically reduces the device resistance enabling the resistance-switching behavior in the subsequent cycles for the filamentary regime [26]. The forming process directly impacts the lifespan, forming yield, and C2C variability of the memristor. After forming, *set* and *reset* operations can be applied, which bring the device to the Low Resistive State (LRS) and High Resistive State (HRS), respectively [27].

The authors of [28] compared three forming algorithms: Single pulse, Incremental Form (IF), and Incremental Form and Verify (IFV). The first method applies a single voltage pulse for forming memristors, the second one applies multiple voltage pulses with increasing magnitudes, and the third, IFV, involves increasing voltage pulses combined with verification steps to monitor the state of the cell and to prevent current overshoots. They have found out that IFV outperforms the other techniques in terms of cell yield and switching behavior due to the tight control of the conductive filament creation.

In this work, the Incremental Step Pulse Program and Verify Algorithm (ISPVA) [29], an IFV algorithm, is used. The algorithm, illustrated in Fig. 1, applies voltage pulses with increasing magnitude to the electrodes to change the resistive state. After each programming pulse V_{prog} , a verification voltage V_{verify} is applied to measure if the desired current has been reached. The algorithm contains adjustable parameters, e.g., the pulse duration T_{pulse} , the start voltage V_{start} , the voltage increase V_{step} , and the stop voltage V_{stop} . During *set*, positive voltages are applied to the Word Line (WL) and 0 V to the Bit Line (BL). During *reset*, positive voltages are applied to the BL and 0 V to the WL.

ReRAMs: Structure and Metrics

In 1T1R crossbars, each ReRAM cell consists of one transistor and one memristive device. The transistor is used as a switch to disconnect the memristor from the crossbar,

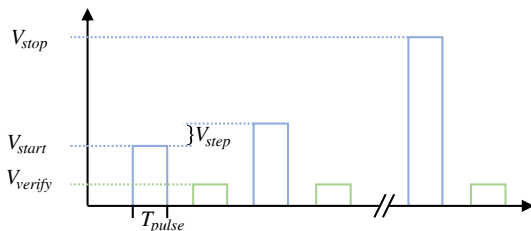


Fig. 1: ISPVA [29] voltage sequence

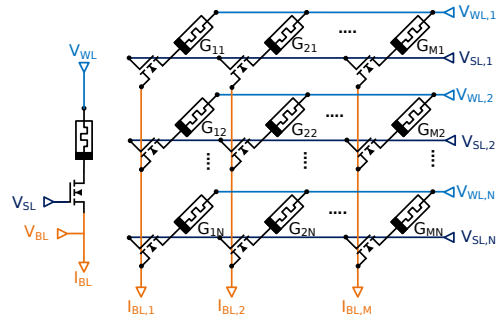


Fig. 2: 1T1R crossbar (pseudo crossbar)

which reduces sneak-path currents [30]. There are three types of 1T1R crossbars, namely *typical*, *vertical*, and *pseudo* crossbars [31]. They differ in the horizontal or vertical placement of the Source Line (SL), WL, and BL. The conductance value of the memristor G_{ij} represents the weight. The read voltage applied to the WL represents the input, and the output current at the BL corresponds to the result of the Matrix-Vector Multiplication (MVM) between the weights and inputs. The SL is connected to the gate of the transistor. Fig. 2 shows a pseudo crossbar, which is used later in the case study. In pseudo crossbars, WL and SL are both placed in the horizontal direction. The following properties are typically analyzed to characterize a ReRAM cell:

- **Window Margin:** $R_{\text{OFF}}/R_{\text{ON}}$ ratio.
- **Retention:** Stability of the cell (at higher temperatures).
- **Endurance:** Maximum number of programming cycles N_{cmax} at a constant Window Margin (WM).
- **Read disturb:** Resistance-drifts after multiple readouts.
- **Variation:** C2C variation (different cycles) and D2D variation (different devices).

Different physical compositions of the ReRAM cells result in varying behaviors. $\text{MO}_x/\text{CuTe}_x$ shows a good retention, while $\text{HfO}_2/\text{CuTe}_x$ reports large WMs at a high endurance. HfO_2/Ti present a good trade-off between endurance and retention [32]. Related works have also revealed that programming algorithms impact the switching behavior [33], variability, and reliability [16], [34]. Further, the read voltages have significant effects on read disturb and C2C variation. The authors of [17] analyzed this for $\text{Pt}/\text{ZrO}_2/\text{Ta}/\text{Pt}$ cells. They have found out that it is advantageous to read in the *reset* direction. In the following study, we plan to examine this phenomenon for HfO_2/Ti cells. A particular focus is placed on the HRS since a gradual HRS drift towards the LRS is observed over cycling for this cell type [35]. When N_{cmax} is exceeded, programming the HRS becomes unfeasible, i.e., the cell is broken.

The NeuroBreakoutBoard (NBB)

The aim of NBB is to provide a customizable infrastructure for measuring Non-Volatile Memories (NVM) [24]. The NBB includes a configurable interconnect matrix and circuitry for voltage pulse generation and current measurement. These components are explained in more detail in the following.

1) *Configurable Signal Interconnection Module*: The board employs arrays of multiplexers to distribute different signal lines or ground potential to each pin of the NVM socket independently. Around the socket, 68 8:1 multiplexers are spread over the four sides of the socket (see Fig. 3). Each multiplexer receives 5 signals from the Digital-to-Analog Converter (DAC), a ground line, and an external voltage line. The south multiplexers are additionally connected to the current sensing module.

2) *Voltage Pulse Generator Module*: A 12-bit, 16-channel DAC is used to generate the different voltage levels needed for the crossbar operations. The 16 channels can be used independently. Programming ReRAM cells requires very short and precise voltage pulses [29]. For this purpose, additional analog switches with switching times below 60 ns are provided.

3) *Current Sensing Module*: Accurate current sensing is required for different tasks like reading the calculation result of a MVM. Furthermore, programming algorithms, such as ISPVA, constantly require accurate feedback about the current. The currents can be measured at the BLs of the crossbar (see Fig. 2). For accurate sensing, the NBB has a circuit called TIA sense, which uses adjustable feedback resistors to translate currents into voltages. The NBB has 16 TIA sense circuits, one for each south pin. To measure a wide range of currents, different feedback resistances from 43 Ω to 100 k Ω can be used. TIA sense further includes an amplifier to adjust the voltage for the Analog-to-Digital Converter (ADC). The ADC has 8 18-bit channels, which can be used simultaneously. The input resistance is 1 M Ω .

The authors of [24] evaluated the measurement accuracy of the NBB. For measuring crossbar cells, we expect the resistances to range from 1 k Ω to 100 k Ω . In this range, the measurement accuracy remains highly reliable, with a relative error of less than 0.5 %.

III. THE PROPOSED CONTROLLER BOARD AND INTERFACE

The main components of the controller board developed in this paper are shown in Fig. 3. It can be plugged into the FPGA Mezzanine Card (FMC) connector of the NBB. In general terms, the controller board generates the control signals for the NBB modules. The STM32 microcontroller manages the configurable signal interconnection module, the voltage pulse generator module, and the current sensing module. In Fig. 3,

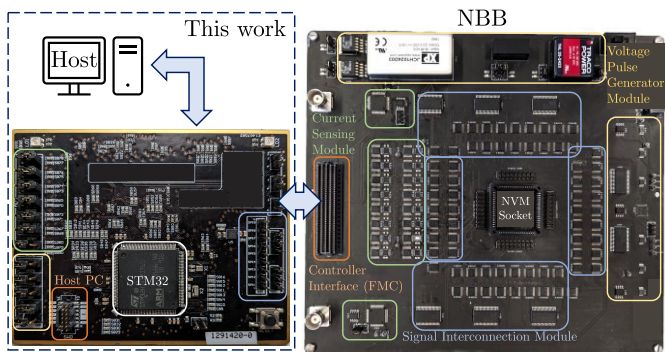


Fig. 3: Integration of NBB into automated measuring system

the control parts are highlighted in the same color as the corresponding modules of the NBB. All interfaces (host PC - controller board - NBB) are marked in orange. The controller board enables the communication between the host PC and the NVM chip. To be more precise, the developed board

- controls the multiplexers for each operation to connect the lines to the BLs, WLs, and SLs of the NVM (blue).
- implement ReRAM programming algorithms such as ISPVA by controlling the DAC and analog switches. The voltage pulses must have different amplitudes, shapes, and polarities depending on the operation and the underlying technology (yellow).
- control the feedback resistors and the TIA for accurate voltage sensing (green).

Host PC to Control Board Communication

For communication between the host PC and the control board, a Universal Asynchronous Receiver/Transmitter (UART) interface with Protocol Buffer (Protobuf) for message serialization is used. Before any command can be sent to the control board, the setup phase of the controller must be completed to initialize the SPI channels, the clock, and the GPIO interface. Then the NBB is set up, i.e., the IO expanders are woken up, the DAC is cleared, the ADC converter is initialized, the multiplexer arrays are reset by switching them to ground potential, and the feedback resistors of the TIAs are set to their highest values.

After the setup phase, the main loop starts on the microcontroller (see Fig. 4). `Receive Request` checks the host PC's request for validity and unpacks the message. If the operation is valid, it will be executed on the NVM chip in `Process Command`. Finally, the result of the operation is sent back to the host PC in `Send Response`. For example, this is the measured current of a read operation.

Python API

To abstract the Protobuf format and UART messages for the user, we developed a host-side Application Programming Interface (API). It is a set of Python functions that can be called to access the NVM cells. A sample of the API functions is shown in Fig. 5. The corresponding cell can be selected with `sl` and `bl`. Note that all API functions have a return value which is received by `Send Response` (for the sake of clarity, this is not shown here). These Python functions were also used to conduct the measurements presented in the case study in Section IV.

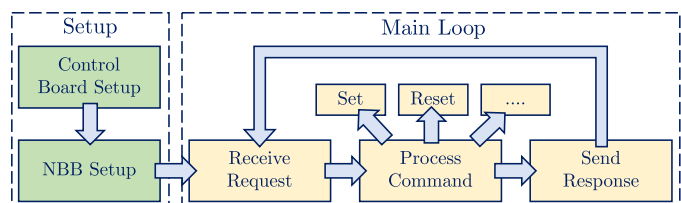


Fig. 4: Setup and main loop of the control board

IV. VALIDATION OF THE PROPOSED CONTROLLER BOARD AND INTERFACE

To properly validate the proposed controller board and interface, we conduct a case study using a 12×7 TiN/Ti/HfO₂/TiN pseudo crossbar. We evaluate the C2C variation, read disturb, and endurance as metrics (see Section II). The crossbar is plugged into the NBB's socket. The ReRAM devices are formed using the ISPVA [29] and the parameters provided by the vendor. After applying a *forming-reset-set* sequence to all cells, the C2C variation and the read disturb of the LRS and HRS are analyzed. In the following, the ISPVA algorithm is also used to program the LRS and HRS (see Section II). Table I lists all relevant parameters.

A. Cycle-To-Cycle Variation

We analyze the C2C variation for different *read* voltages, i.e., WL voltages (see Fig. 2). We apply negative and positive *read* voltages, specifically -0.3 V, -0.25 V, -0.2 V, -0.15 V, -0.1 V, 0.1 V, 0.15 V, 0.2 V, 0.25 V, and 0.3 V. For each WL voltage, we apply the *set-read-reset-read* sequence 100 times and measure the SL current using the measurement circuitry of the NBB (see Section III).

The results for two different cells are shown in Fig. 6. The Cumulative Distribution Function (CDF) of the LRS and HRS for the same WL voltage share the same color. In all measurements, both LRS and HRS show a higher C2C variance at higher WL voltages (in terms of absolute value). It can be seen that the measured currents in the HRS have a smaller variance for negative WL voltages (Figs. 6a and 6c) than for positive ones (Figs. 6b and 6d). The higher the (positive) WL voltage, the more likely the HRS swings towards LRS when reading. This is because the *read* operation with positive voltages has the same polarity as the *set* operation (see Table I).

The same behavior has been described by the authors of [17]. They suggest reading in the *reset* direction because it

results in a slower transition of the resistance state, as opposed to reading in the *set* direction. Additionally, employing lower voltages enhances the resistance stability.

B. Read Disturb

Since a major application of ReRAM crossbars is the inference of NNs, it is important to evaluate the read disturb, which refers to the alteration of data caused by read operations. A major advantage of CIM is that the weights, represented as LRS and HRS, are programmed only once and then used for multiple inferences. Therefore, the cells must remain stable even when read several times. We analyze the read disturb for the WL voltages mentioned in Section IV-A. For each of the 10 WL voltages, we apply the sequence *set-read(100)-reset-read(100)*, 50 times, i.e., 1,000 *write* operations and 100,000 *read* operations are performed per cell.

Fig. 7 shows the read stability of a stable and an unstable cell. Positive BL currents occur as a result of positive WL voltages and negative currents as caused by negative WL voltages. For clarity, only every 10th read cycle is shown. The box plots illustrate the variation of 50 independent measurements. The box boundaries represent the 25% and 75% quartiles. The lower and upper whiskers denote the 2.5% and 97.5% boundaries, respectively. The median is highlighted in orange, and the dashed lines connect the mean values. The HRS is always the state closer to the x-axis (see also Fig. 6). We show results for cells with a stable (Fig. 7a) and unstable (Fig. 7b) HRS. For both cases, negative read voltages, i.e., voltages in the *reset* direction, are preferred. In cells with an unstable HRS, the cell is continuously reprogrammed and switches to the LRS after just a single-digit read operation. This effect becomes more pronounced with higher WL voltages. As seen in the example from Fig. 7b, HRS and LRS states significantly overlap with positive WL voltages after only 10 read accesses. For read operations with negative WL voltages, all states remain distinguishable after 50 accesses. Despite separable states, the high variance in HRS can harm computing operations.

The maximum endurance of a particular ReRAM technology depends on the maximum programming energy the system can endure before failure [32]. This means that each *set* and *reset* operation contributes to the gradual degradation of the oxide material, leading to failure at N_{cmax} . The reported maximum endurance for Oxide-based Random Access Memory (OxRAM) technology has been documented within the range of 10^3 to 10^9 cycles [32]. In the case of HfO₂/Ti cells, oxide degradation primarily impacts the HRS, resulting in a gradual drift of the HRS towards the LRS [35]. This explains the behavior observed in Fig. 7b. The observed N_{cmax} values of the tested crossbar exhibited significant variability among different cells. While some cells have a small N_{cmax} of 100 measurements, others show a stable HRS even after 10,000 cycles.

```

formCell(..., s1, b1, vGate=1.8,
           iTargetSet=80, vGateRead=1.5)
resetCell(..., s1, b1, vGateReset=2.7,
            iTargetReset=5, vGateRead=1.5)
setCell(..., s1, b1, vGate=1.5,
          iTarget=80, vGateRead=1.5)
readCell(..., s1, b1, vGateRead=1.5,
           vRead=vRead)

```

Fig. 5: Extract of API functions

TABLE I: ISPVA *set* and *reset* parameters

Parameter	Value
Top-electrode voltage LRS (V_{te})	0.5 V : 0.1 V : 2 V
Gate voltage LRS ($V_{g,lrs}$)	1.5 V
Current target LRS ($I_{trg,lrs}$)	80.0 μ A
Bottom-electrode voltage HRS (V_{be})	0.5 V : 0.1 V : 2 V
Gate voltage HRS ($V_{g,hrs}$)	2.7 V
Current target HRS ($I_{trg,hrs}$)	5.0 μ A

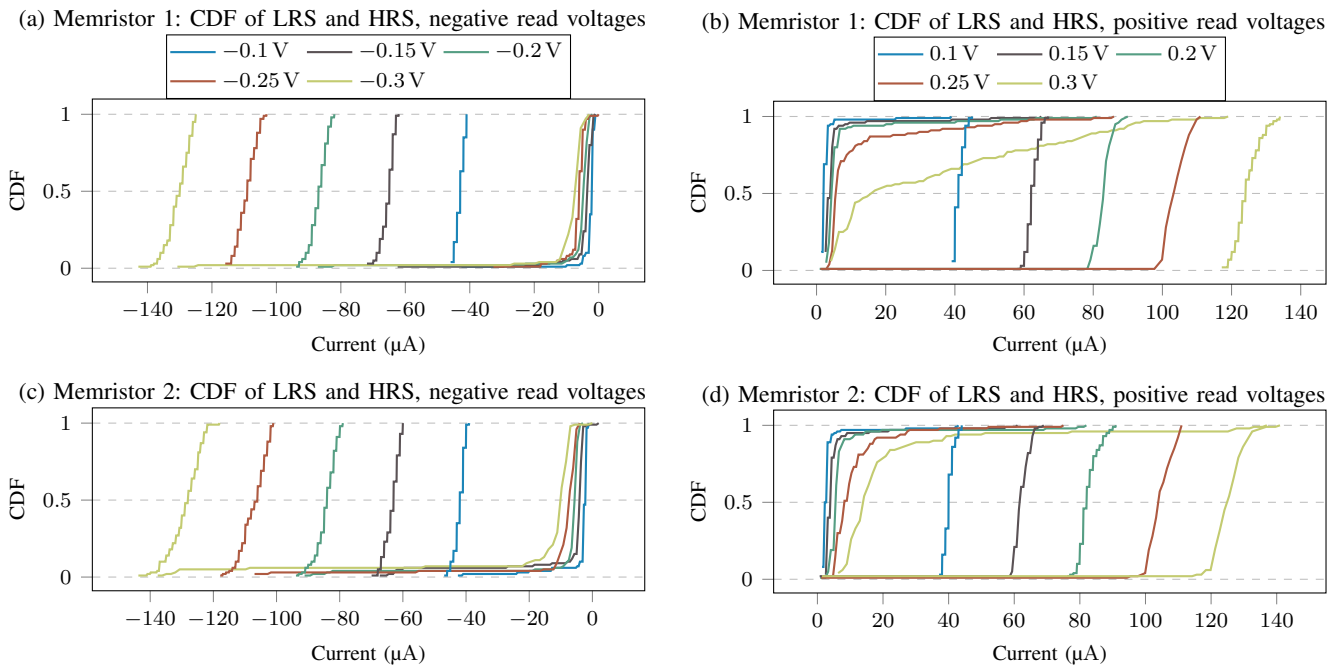


Fig. 6: CDF of LRS and HRS states for different cells using negative read voltages (left) vs. positive read voltages (right).

V. CONCLUSION

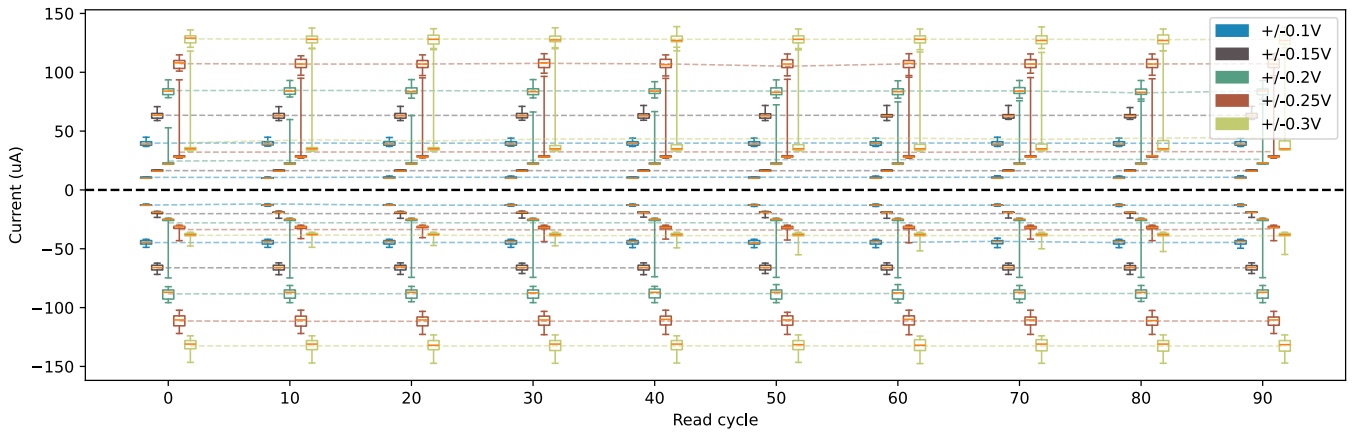
In this work, we developed a fully automated test platform to characterize ReRAM cells in 1T1R crossbar arrays. We implemented a control board that enables communication between a host PC and the NBB. Using our Python-based API, we are able to automate test cases for cell measurements.

The proposed controller board and interface were validated in a case study. More specifically, we analyzed the effect of read voltages on C2C variation and read disturb in TiN/Ti/HfO₂/TiN cells. The findings reveal that reading in *reset* direction achieves better results, especially for the read disturb, as reading in *set* direction tends to swing the HRS towards the LRS.

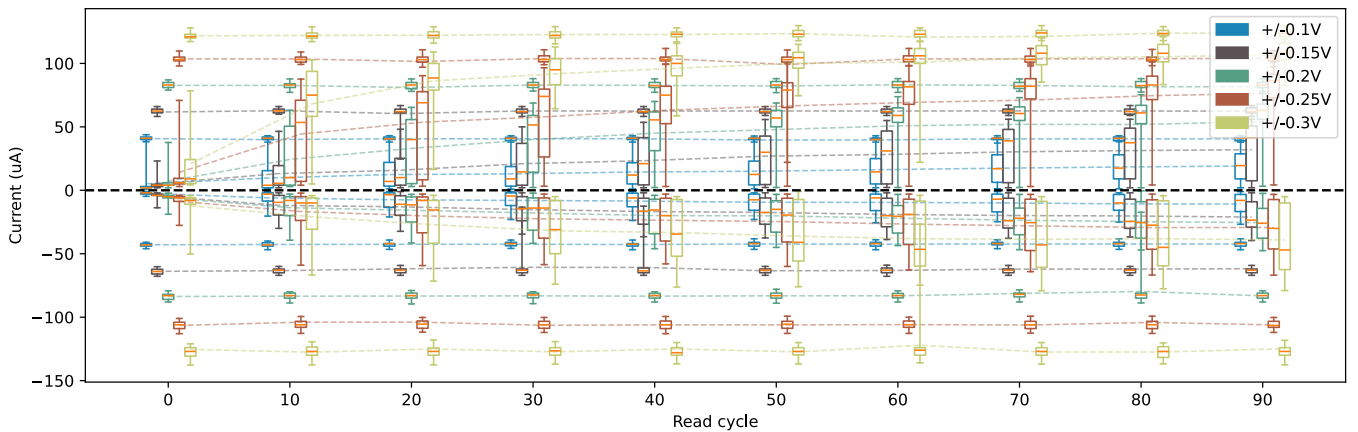
Finally, this work optimizes laboratory measurement procedures, offering considerable time savings. Cell measurements, which may span several hours, can now be conducted without continuous supervision. Additionally, automated measurements ensure the consistency of data collection by adhering to predefined and standardized procedures, minimizing variations and human errors. Looking ahead, the next steps are to add support for MVMs and to automate test cases for multi-bit measurements.

REFERENCES

- [1] X. Zou, S. Xu, X. Chen, L. Yan, and Y. Han, "Breaking the von Neumann bottleneck: architecture-level processing-in-memory technology," *Science China Information Sciences*, vol. 64, no. 6, p. 160404, 2021.
- [2] X. Huang, C. Liu, Y.-G. Jiang, and P. Zhou, "In-memory computing to break the memory wall," *Chinese Physics B*, vol. 29, no. 7, p. 078504, 2020.
- [3] S.-T. Wei, B. Gao, D. Wu, J.-S. Tang, H. Qian, and H.-Q. Wu, "Trends and challenges in the circuit and macro of RRAM-based computing-in-memory systems," *Chip*, vol. 1, no. 1, p. 100004, 2022.
- [4] A. Baroni, A. Glukhov, E. Pérez, C. Wenger, D. Ielmini, and C. Zambelli, "An energy-efficient in-memory computing architecture for survival data analysis based on resistive switching memories," *Frontiers in Neuroscience*, 2022.
- [5] J. Hazra, M. Liehr, K. Beckmann, M. Abedin, S. Rafiq, and N. Cady, "Optimization of Switching Metrics for CMOS Integrated HfO₂ based RRAM Devices on 300 mm Wafer Platform," in *2021 IEEE International Memory Workshop (IMW)*. IEEE, 2021, pp. 1–4.
- [6] J. S. Meena, S. M. Sze, U. Chand, and T.-Y. Tseng, "Overview of emerging nonvolatile memory technologies," *Nanoscale research letters*, 2014.
- [7] J. S. Vetter and S. Mittal, "Opportunities for nonvolatile memory systems in extreme-scale high-performance computing," *Computing in Science and Engineering*, 2015.
- [8] N. Raghavan *et al.*, "Stochastic variability of vacancy filament configuration in ultra-thin dielectric RRAM and its impact on OFF-state reliability," in *2013 IEEE International Electron Devices Meeting*, 2013.
- [9] H.-S. P. Wong *et al.*, "Metal-oxide RRAM," *Proceedings of the IEEE*, 2012.
- [10] S. Yu, X. Guan, and H.-S. P. Wong, "On the stochastic nature of resistive switching in metal oxide RRAM: Physical modeling, Monte Carlo simulation, and experimental characterization," in *2011 International Electron Devices Meeting*. IEEE, 2011.
- [11] E. Brum *et al.*, "Evaluating the Impact of Process Variation on RRAMs," in *LATS*. IEEE, 2021.
- [12] Y. Fang *et al.*, "Improvement of HfO_x-based RRAM device variation by inserting ALD TiN buffer layer," *IEEE Electron Device Letters*, 2018.
- [13] W. Wu *et al.*, "A methodology to improve linearity of analog RRAM for neuromorphic computing," in *2018 IEEE symposium on VLSI technology*. IEEE, 2018.
- [14] T. Kempen, R. Waser, and V. Rana, "50x Endurance improvement in TaOx RRAM by extrinsic doping," in *IMW*. IEEE, 2021.
- [15] H. Liu *et al.*, "Uniformity improvement in 1T1R RRAM with gate voltage ramp programming," *IEEE Electron Device Letters*, 2014.
- [16] A. Baroni, C. Zambelli, P. Olivo, E. Pérez, C. Wenger, and D. Ielmini, "Tackling the Low Conductance State Drift through Incremental Reset and Verify in RRAM arrays," in *IIRW*. IEEE, 2021.
- [17] C. Bengel *et al.*, "Reliability aspects of binary vector-matrix-multiplications using ReRAM devices," *Neuromorphic computing and engineering*, 2022.
- [18] L. Xia, M. Liu, X. Ning, K. Chakrabarty, and Y. Wang, "Fault-tolerant



(a) Read stability for cells with stable HRS



(b) Read stability for cells with unstable HRS

Fig. 7: Read stability for different ReRAM cells using different read voltages

- training with on-line fault detection for RRAM-based neural computing systems,” in *DAC*, 2017.
- [19] L. Xia *et al.*, “Stuck-at fault tolerance in RRAM computing systems,” *IEEE JETCAS*, 2017.
- [20] L. Chen *et al.*, “Accelerator-friendly neural-network training: Learning variations and defects in RRAM crossbar,” in *DATE*. IEEE, 2017.
- [21] R. Berdan, A. Serb, A. Khiat, A. Regoutz, C. Papavassiliou, and T. Prodromakis, “A μ -Controller-Based System for Interfacing Selectorless RRAM Crossbar Arrays,” *IEEE Transactions on Electron Devices*, 2015.
- [22] J. Cayo and I. Vourkas, “Design Steps towards a MCU-based Instrumentation System for Memristor-based Crossbar Arrays,” in *MOCAS*. IEEE, 2021.
- [23] R. De La Fuente, I. Vourkas, and M. Perez, “On the Development of MCU-based ad hoc HW Interface Circuitry for Memristor Characterization,” in *ECCTD*. IEEE, 2020.
- [24] F. Staudigl *et al.*, “Work-in-Progress: A Universal Instrumentation Platform for Non-Volatile Memories,” in *ESWEEK*, 2023.
- [25] Guitarra, Silvana and Trojman, Lionel and Raymond, Laurent, “Resistive Switching Model of OxRAM Devices Based on Intrinsic Electrical Parameters,” in *2019 Latin American Electron Devices Conference (LAEDC)*, 2019.
- [26] L. B. Poehls *et al.*, “Review of Manufacturing Process Defects and Their Effects on Memristive Devices,” *Journal of electronic testing*, 2021.
- [27] F. M. Puglisi, P. Pavan, A. Padovani, and L. Larcher, “A study on HfO₂ RRAM in HRS based on I–V and RTN analysis,” *Solid-State Electronics*, 2014.
- [28] A. Grossi *et al.*, “Electrical characterization and modeling of pulse-based forming techniques in RRAM arrays,” *Solid-State Electronics*, vol. 115, pp. 17–25, 2016.
- [29] E. Perez, C. Zambelli, M. K. Mahadevaiah, P. Olivo, and C. Wenger, “Toward Reliable Multi-Level Operation in RRAM Arrays: Improving Post-Algorithm Stability and Assessing Endurance/Data Retention,” *IEEE Journal of the Electron Devices Society*, 2019.
- [30] M. Mao, Y. Cao, S. Yu, and C. Chakrabarti, “Optimizing Latency, Energy, and Reliability of 1T1R ReRAM Through Cross-Layer Technique,” *IEEE Journal on Emerging and Selected Topics in Circuits and Systems*, 2016.
- [31] S. Son, C. La Torre, A. Kindsmüller, V. Rana, and S. Menzel, “A Study of the Electroforming Process in 1T1R Memory Arrays,” *IEEE Transactions on Computer-Aided Design of Integrated Circuits and Systems*, 2022.
- [32] C. Nail *et al.*, “Understanding RRAM endurance, retention and window margin trade-off using experimental results and simulations,” in *2016 IEEE International Electron Devices Meeting (IEDM)*. IEEE, 2016.
- [33] E. Perez, M. K. Mahadevaiah, E. P.-B. Quesada, and C. Wenger, “Variability and energy consumption tradeoffs in multilevel programming of RRAM arrays,” *IEEE Transactions on Electron Devices*, vol. 68, no. 6, pp. 2693–2698, 2021.
- [34] A. Baroni *et al.*, “Low Conductance State Drift Characterization and Mitigation in Resistive Switching Memories (RRAM) for Artificial Neural Networks,” *IEEE Transactions on Device and Materials Reliability*, 2022.
- [35] G. Sassine *et al.*, “Optimizing Programming Energy for Improved RRAM Reliability for High Endurance Applications,” in *2018 IEEE International Memory Workshop (IMW)*. IEEE, 2018.